International Scientific Conference 20 UNITECH 26

INTERNATIONAL SCIENTIFIC CONFERENCE
19-21 November 2026
GABROVO

TOPOLOGY-OPTIMISED WEB OPENINGS IN AN S355 I-BEAM: PLASTIC LOAD-CARRYING BEHAVIOUR, MANUFACTURABLE DESIGNS AND COST

Gürkan İRSEL[1,*]

[1]*Trakya University, Faculty of Engineering, Department of Mechanical Engineering, Edirne 22100, Türkiye*

**Corresponding author: gurkanirsel@trakya.edu.tr*

Abstract

Topology optimisation based on the finite element method is widely used to reduce the weight of beams subjected to bending, but it is formulated for linear elastic behaviour; the plastic capacity of the lightened beam and the cost of manufacturing the layout are rarely examined together. An S355 IPE100 beam (500 mm, three-point bending) was optimised with SIMP (solid isotropic material with penalisation), which divides the beam into cells and seeks the stiffest distribution for a given amount of material, with the flanges kept (A) or free (B). The layouts were analysed in ANSYS with large displacement and plasticity up to 12 mm at mid-span. Under the loading and load-strip model studied, the largest computed reaction force of the solid beam is 93.9 kN; the design B60, 40 % lighter, reached 99 % of it (92.7 kN) and the design A50, 18 % lighter, 74 % (70.0 kN). A manufacturable design was derived from each layout: an IPE100 with seven laser-cut web openings (F-A, 3.49 kg, 77.4 kN) and a tapered girder welded from three plates (F-B, 2.51 kg, 90.9 kN). The force per unit mass of F-A is close to that of the solid beam (22.2 and 23.2 kN/kg) and that of F-B is 56 % higher (36.2 kN/kg).

Keywords: Topology Optimisation, SIMP, I-Beam, Web Openings, Plasticity, Laser Cutting, Cost

INTRODUCTION

The web of a rolled I-section is often thicker than the shear force between the support and the load requires. Castellated and cellular beams make use of this: web openings reduce the mass, while cutting and re-welding increase the section depth. A cellular beam needs two cuts along the web, which increases the fabrication cost and the waste [1]. For large openings, the critical mechanism of perforated beams is Vierendeel bending (separate bending of the short T-sections above and below an opening). It has been studied for eleven opening shapes with nonlinear finite elements [2], and elliptically based opening shapes have been optimised with a model validated by experiments [3].

Topology optimisation places material in a design domain by minimising an objective under constraints. Its roots are the homogenisation method [4] and the material distribution formulation with density variables [5]; the SIMP (solid isotropic material with penalisation) interpolation [5,6] is widely used, and the approaches have been compared [7]. In SIMP the elastic modulus of each element is scaled by its density raised to a power $p > 1$; intermediate densities are thereby penalised, and the solution tends towards a solid–void distribution [5,6]. Density filters suppress checkerboard patterns and mesh dependence [8,9], and short codes make the method reproducible [10,11,12].

The method has been applied to steel I-sections with openings; the optimised beams showed a higher load capacity and a lower stress intensity than conventional cellular beams, and the authors listed the practical limits of routine use [13,14]. It has also been used for vehicle parts: an engine mount bracket under dynamic load [15], diesel engine parts [16], a lattice-embedded

This is an open access article licensed under Creative Commons Attribution 4.0 International
Print ISSN: 1313-230X, Online ISSN: 3033-1404

brake pedal (about 27 % mass reduction) [17], a suspension cap (35 % mass reduction) [18] and a suspension arm [19]; the topology design of vehicle components [20] and the combination of topology and shape optimisation with neural networks [21] have also been reported.

Formulations beyond linear compliance exist: geometric nonlinearity [22,23], elastoplasticity [24,25], stress criteria [26] and buckling constraints [27]. For geometrically nonlinear structures, designs obtained with a linear and a nonlinear model usually have similar stiffness, but the difference grows where buckling or snap-through occurs [22]. Layouts from a stress-constrained formulation carried more load up to yielding than minimum-compliance layouts [25].

Topology optimisation of I-beams has mostly been evaluated in terms of linear elastic stiffness and stress; the behaviour of the resulting layouts in the plastic range, their conversion into manufacturable geometry and their cost have rarely been considered together. In this study these three steps are combined in one application algorithm for the same beam. The first aim of the study is to determine how the plastic (permanent deformation) load-carrying behaviour of an I-beam lightened by topology optimisation changes compared with the solid beam. The second aim is to determine the extra cost of actually manufacturing the resulting layout relative to the solid beam. For this purpose, a 500 mm IPE100 beam of S355 steel was optimised in three-point bending with SIMP (flanges kept or free), the layouts were analysed in ANSYS with large displacement and plasticity up to 12 mm, and laser-cut manufacturable designs were derived from two layouts, analysed and costed.

2. MATERIALS AND METHODS

2.1. Application Algorithm

The application algorithm followed in this study is given in Figure 1. It consists of four stages: linear topology optimisation, elastoplastic analysis of the layouts and comparison with the solid beam, derivation and analysis of manufacturable designs, and calculation of the extra manufacturing cost. The algorithm contains three checks: the optimisation is stopped when the largest density change falls below 0.01 or after 100 iterations; the nonlinear results are checked with a refined mesh; and the manufacturable designs are arranged with straight edges, corner radii of at least 4 mm and ligaments of at least 8 mm.

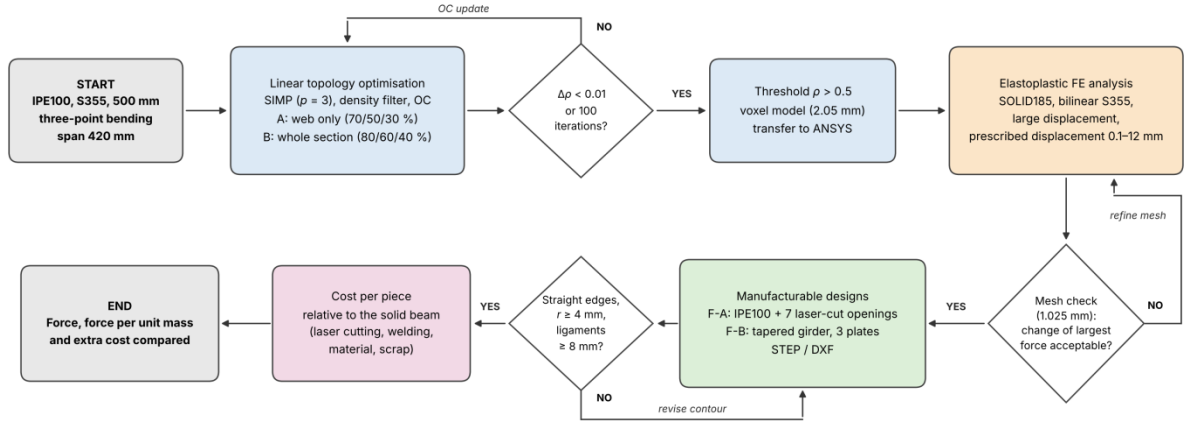


Fig. 1. *Application algorithm: topology optimisation, elastoplastic analysis, manufacturable design and cost.*

In the text, the IPE100 without openings is called the solid beam. Compliance is the work done by the load and measures the flexibility of the structure under load; a small compliance means a stiff structure. The optimisation was carried out in two setups: in setup A the flanges are kept and only the web is optimised, in setup B the

whole section including the flanges is optimised. The number in a design name is the percentage of material retained; for example, 50 % of the web material remains in A50 and 60 % of the total material in B60 (A70, A50, A30, B80, B60, B40). The manufacturable designs with straight edges derived from A50 and B60 are called F-A and F-B. The largest force is the highest value of the force–displacement curve, the force per unit mass (kN/kg) is the largest force divided by the mass of the beam, and ε_{p} denotes the equivalent plastic strain.

2.2. Mathematical Formulation of the Topology Optimisation

Problem: The design domain Ω is discretised into n hexahedral elements of volume v_e. Each element carries a design variable ρ_e between a small lower bound $\rho_{\min}$ and 1. The compliance minimisation problem with a volume constraint reads

$$\begin{aligned} &\min c(\rho) = f^{\mathrm{T}}u \quad \text{subject to} \quad K(\tilde{\rho})u = f, \\ &\sum\nolimits_e v_e \tilde{\rho}_e \le V^*, \qquad \rho_{\min} \le \rho_e \le 1 \end{aligned} \tag{1}$$

where u is the displacement vector, f the load vector, K the global stiffness matrix, $\tilde{\rho}$ the filtered density and V^* the allowed volume. Compliance is twice the strain energy of the structure, so that minimising c maximises the stiffness for the given load.

SIMP Interpolation: The Young's modulus of element e is interpolated between a void value $E_{\min}$ and the solid value E_0 with the penalisation exponent p,

$$\begin{aligned} &E_e(\tilde{\rho}_e) = E_{\min} + \tilde{\rho}_e^{\,p}(E_0 - E_{\min}), \\ &K = \sum\nolimits_e E_e(\tilde{\rho}_e)K_e^0, \qquad K_e^0 = \int B^{\mathrm{T}} D^0 B \,\mathrm{d}V \end{aligned} \tag{2}$$

Here B is the strain–displacement matrix of the eight-node element, D^0 the elasticity matrix for unit modulus, and K_e^0 is evaluated with 2 × 2 × 2 Gauss points. The values $p = 3$, E_0 = 210 GPa and $E_{\min} = 10^{-6}E_0$ were used (Figure 3a). The penalisation makes intermediate densities inefficient and drives the design towards 0 and 1 [5].

Density Filter: The density filter replaces each design variable by a weighted average of its neighbours within the radius $r_{\min}$,

$$\begin{aligned} \tilde{\rho}_e &= \frac{\sum_i w_{ei} v_i \rho_i}{\sum_i w_{ei} v_i}, \\ w_{ei} &= \max(0,\, r_{\min} - d_{ei}) \end{aligned} \tag{3}$$

where d_{ei} is the distance between the centres of elements e and i (Figure 3b). The filter introduces a minimum length scale of the order of $r_{\min}$ and removes checkerboard patterns and mesh dependence [8,9]. The weight matrix is assembled once with a k-d tree.

Sensitivities. The compliance depends on ρ through $K(\tilde{\rho})$ only. Differentiating the equilibrium equation $Ku = f$ with respect to $\tilde{\rho}_e$ gives $(\partial K/\partial \tilde{\rho}_e)u + K\,\partial u/\partial \tilde{\rho}_e = 0$, hence $\partial u/\partial \tilde{\rho}_e = -K^{-1}(\partial K/\partial \tilde{\rho}_e)u$. Because f does not depend on ρ and K is symmetric,

$$\begin{aligned} \frac{\partial c}{\partial \tilde{\rho}_e} &= f^{\mathrm{T}}\frac{\partial u}{\partial \tilde{\rho}_e} = -u^{\mathrm{T}}\frac{\partial K}{\partial \tilde{\rho}_e}u \\ &= -p\,\tilde{\rho}_e^{\,p-1}(E_0 - E_{\min})u_e^{\mathrm{T}}K_e^0 u_e \end{aligned} \tag{4}$$

where u_e collects the 24 displacements of element e. Equation 4 is the (negative) element strain energy scaled by the penalisation, and it requires one solution of the equilibrium problem per iteration because the problem is self-adjoint. The chain rule through the filter gives the sensitivities with respect to the design variables,

$$\begin{aligned} \frac{\partial c}{\partial \rho_j} &= \sum\nolimits_e \frac{w_{ej} v_j}{\sum_i w_{ei} v_i}\frac{\partial c}{\partial \tilde{\rho}_e}, \\ \frac{\partial V}{\partial \rho_j} &= \sum\nolimits_e \frac{w_{ej} v_j}{\sum_i w_{ei} v_i} v_e \end{aligned} \tag{5}$$

The sensitivities of the volume have the same form because V depends on the filtered densities.

Update of the Design Variables: The first-order optimality conditions of Eq. 1 for an element with $\rho_{\min} < \rho_e < 1$ state that $-\partial c/\partial \rho_e = \lambda\, \partial V/\partial \rho_e$, where λ is the Lagrange multiplier of the volume constraint. The optimality-criteria (OC) update multiplies each variable by the square root of the ratio of the two sides and limits the step by a move limit m,

$$\rho_e^{\text{new}} = \min\left(1,\ \rho_e + m,\ \max\left(\rho_{\min},\ \rho_e - m,\ \rho_e \sqrt{\frac{-\partial c/\partial \rho_e}{\lambda\, \partial V/\partial \rho_e}}\right)\right) \tag{6}$$

with $m = 0.2$. The multiplier λ is found by bisection so that the filtered volume equals V^* (relative tolerance 10^{-4} on the bracket). Elements in frozen zones (the load strip, the support strips and, in variant A, the flanges) keep $\rho = 1$. The iteration stops when the largest change of a design variable is below 0.01 after at least 30 iterations, or after 100 iterations (Figure 2).

Discretisation and Solution: The beam is discretised with 2.05 mm voxels (60 512 elements, 85 750 nodes, 257 250 degrees of freedom). The stiffness matrix is assembled in coordinate format from the element matrices, the supports are eliminated, and the system is solved with the PARDISO direct solver. The solution of one equilibrium problem takes about 9 s on the workstation (several runs in parallel), and the dominant memory consumption is the factorisation of K.

Verification: The sensitivity expression (Eq. 4) was checked against central finite differences on a coarser model (5 mm voxels, 4 000 elements, random densities between 0.3 and 1). For twelve randomly chosen elements the maximum relative difference was 4.8×10^{-5} with a perturbation of 10^{-5} (Table 1). The stiffness of the voxel model was checked against beam theory: the mid-span deflection of the solid IPE100 under 10 kN is 0.0768 mm in the voxel model (bottom flange, load spread over two node rows) and 0.0787 mm from Timoshenko beam theory, including bending and shear (Eq. 7).

$$\delta = \frac{PL^3}{48EI} + \frac{PL}{4GA_{\text{w}}}, \qquad P_{\text{y}} = \frac{4 f_{\text{y}} W_{\text{el}}}{L}, \qquad P_{\text{p}} = \frac{4 f_{\text{y}} W_{\text{pl}}}{L} \tag{7}$$

Here L is the span, I the second moment of area, A_{w} the web area, W_{el} and W_{pl} the elastic and plastic section moduli, and P_{y} and P_{p} the loads at first yield and at the plastic hinge. These closed-form quantities are used as references for the nonlinear results.

Table 1. *Sensitivity check: analytical expression against central differences (5 mm model, 4 000 elements; six of twelve elements shown)*

Element	$\tilde{\rho}$	$\partial c/\partial \tilde{\rho}$ (Eq 4)	$\partial c/\partial \tilde{\rho}$ (finite diff.)	Rel. diff.
2349	0.395	−7.10677	−7.10673	5.7×10^{-6}
131	0.704	−1.98079	−1.98081	1.1×10^{-5}
3182	0.560	−12.59848	−12.59850	9.3×10^{-7}
3586	0.989	−0.40676	−0.40674	2.9×10^{-5}
139	0.650	−0.56556	−0.56553	4.0×10^{-5}
453	0.830	−2.59460	−2.59460	3.7×10^{-7}

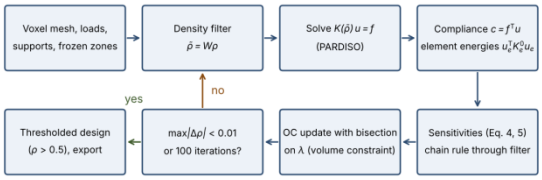


Fig. 2. *Flow of the Topology Optimisation*

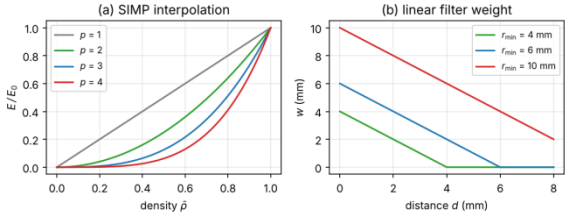


Fig. 3. *SIMP Interpolation (a) and Density Filter (b).*

2.3. Beam, Loading and Numerical Models

Beam and set-up: The beam is a hot-rolled IPE100 of S355 steel, 500 mm long and 4.05 kg in mass (depth 100 mm, flange width 55 mm, web thickness 4.1 mm,

flange thickness 5.7 mm). It rests on two rollers of 30 mm diameter, 40 mm from the ends; a third roller loads the beam at mid-span (span 420 mm; Figure 4).

Material: E = 210 GPa, $\nu = 0.3$ and a yield strength of 355 MPa were taken for S355 [28]. The nonlinear analysis used a bilinear isotropic hardening model (ANSYS TB,BISO) in which the stress increases linearly with plastic strain after yielding; the hardening (tangent) modulus of 2100 MPa ($E/100$) is an assumption.

Closed-form Reference: Closed-form (hand calculation) values: A = 1034 mm^2, I = 171.4 cm^4, W_{el} = 34.28 cm^3, W_{pl} = 39.48 cm^3. They give a first-yield load P_{y} = 115.9 kN, a plastic hinge load P_{p} = 133.5 kN, an elastic stiffness of 127.1 kN/mm and a mid-span deflection of 0.91 mm at first yield (Table 2). The initial stiffness of the finite element model (at 0.1 mm displacement) is 106 kN/mm. It refers to the displacement of the loaded node row and therefore includes the local indentation of the flange under the load, which beam theory does not contain. The linear voxel model of the optimisation gives 130 kN/mm when the deflection is taken at the bottom flange (0.0768 mm under 10 kN; see Verification) and 106–107 kN/mm when it is loaded and evaluated as in the ANSYS model; the difference between the two stiffness values thus arises from the measurement point and the load application, not from the element formulation.

Topology Optimisation Setup: The volume of the beam was divided into small cells (elements), and each cell was given a density between 0 (void) and 1 (solid). The optimisation seeks the density distribution that keeps the beam stiffest for a given amount of material. In setup A the flanges are kept and only the web changes; 70, 50 or 30 % of the web material is retained (A70, A50, A30). In setup B the whole section including the flanges changes; 80, 60 or 40 % of the total material is retained (B80, B60, B40). The material directly under the load and the supports is kept in both setups. The optimisation load is 10 kN, distributed over two node rows of the top flange at mid-span (about 4.1 mm); each support consists of two node rows of the bottom flange (about 4.1 mm). The density filter averages the density of each cell with its neighbours within 6 mm (about three cell lengths), which prevents very thin bars and checkerboard patterns.

Nonlinear Analysis: Cells with a density above 0.5 were taken as solid, and the resulting shape was transferred to ANSYS Mechanical APDL 2020 R1 as eight-node hexahedral elements (SOLID185). The analysis used large displacement and the bilinear material model above. Because of symmetry, half of the beam was modelled (about 24 000–31 000 elements). The load was applied by displacement, not by force: the mid-span displacement of the load strip was increased from 0.1 mm to 12 mm in steps, and the force was obtained from the reactions of the strip. The displacement was prescribed on one node row of the top flange in the mid-span plane, so the loaded width is one element length (about 2.05 mm); each support consists of two node rows of the bottom flange (about 4.1 mm). In the set-up, steel plates are placed between the support rollers and the bottom flange (Figure 4); these plates and the real curved roller contact were not modelled. The loading roller touches the flat flange along a line. According to the Hertz solution [29], the maximum contact pressure of the 15 mm radius roller reaches the yield strength at about 2.8 kN, and first yielding below the surface is expected at about 8 kN; the elastic contact half-width is only 0.53 mm even at 93.9 kN. The contact is therefore plastic over most of the load range and widens; the loaded width of one element length (about 2.05 mm) is an assumption for this widened contact.

Mesh Check: For a mesh check, every element of B60, A50 and F-A was divided into eight (1.025 mm; 144 832 elements for B60 and 198 896 for A50), and the analysis was repeated up to 4 mm.

The computations were run on a workstation with two 10-core Intel Xeon Silver 4114 processors and 31.6 GB of memory. One equilibrium solution of the topology optimisation took about 9 s; the ANSYS and Python processes used 71.4 and 14.4 CPU hours over 14.0 hours of logged work.

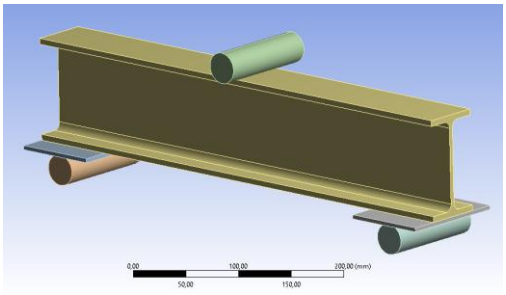


Fig. 4. *Loading arrangement: IPE100 beam on support plates and two rollers (Ø30 mm, 40 mm from the ends) with the loading roller at mid-span (three-point bending, span 420 mm)*

Table 2. Closed-form properties of the IPE100 beam (span 420 mm, S355)

Quantity	Symbol	Value
Cross-section area	A	1034 mm^2
Second moment of area	I	171.4 cm^4
Elastic modulus of section	W_{el}	34.28 cm^3
Plastic modulus of section	W_{pl}	39.48 cm^3
First-yield load	P_{y}	115.9 kN
Plastic hinge load	P_{p}	133.5 kN
Elastic stiffness (bending + shear)	k	127.1 kN/mm
Mid-span displacement at first yield	δ_{y}	0.91 mm

3. TOPOLOGY OPTIMISATION RESULTS

Layouts: Figure 5 shows the layouts found. In setup A, a diagonal truss forms between the load strip and the supports: with 50 % of the web retained (3.33 kg), three triangular openings appear; with 30 % (3.04 kg), the diagonals become thinner and the openings larger. In setup B, the optimisation removes the outer parts of the flanges and the web near the supports; with 80 and 60 % of the material retained (3.24 and 2.43 kg), a fish-belly shape (deep at mid-span, shallow at the ends) forms; with 40 % (1.63 kg), a fan of radial bars appears under the load.

Compliance: The compliance relative to the solid beam (linear elastic) is 1.45 for A50, 2.10 for A30, 1.01 for B80, 1.16 for B60 and 1.71 for B40; B80 is thus almost as stiff as the solid beam. In the final output of the optimisation, the density of some elements is neither 0 nor 1 (between 0.1 and 0.9; referred to here as intermediate-density elements). Their share is 6 % for A50 and 14 % for B40. When the density is thresholded at 0.5, the compliance decreases by 0.4 % (B80) to 12 % (A30, B40).

Filter Radius: With a filter radius of 4 mm instead of 6 mm, the compliance of A50 changes from 1.447 to 1.432 times that of the solid beam, and the share of intermediate-density elements from 6.0 % to 3.9 % (Table 3). The compliance is thus insensitive to the filter radius in this range; all runs stopped at 100 iterations, so the comparison refers to unconverged layouts.

Convergence: The compliance histories (Figure 6) decrease almost steadily. All runs stopped at the limit of 100 iterations, and the largest density change in the last iteration is 0.045–0.16 (stopping criterion 0.01). The layouts obtained are therefore candidate topologies reached in 100 iterations, not exact optima.

Table 3. *Topology optimisation runs: mass of the thresholded design, compliance relative to the solid beam, share of intermediate-density elements (density 0.1–0.9) and the largest density change (Δρ) in the last iteration. Retained: share of the web material in A and of the total material in B; r_{min}: filter radius.*

Design	Retained	$r_{\min}$ (mm)	Mass (kg)	Compliance ratio	Intermediate-density elements (%)	Largest Δρ in last iteration
A70	web 70 %	6	3.67	1.127	7.2	0.045
A50	web 50 %	6	3.33	1.447	6.0	0.101
A30	web 30 %	6	3.04	2.099	7.3	0.106
A50r4	web 50 %	4	3.34	1.432	3.9	0.162
A50r10	web 50 %	10	3.35	1.465	9.9	0.068
B80	volume 80 %	6	3.24	1.015	5.3	0.067
B60	volume 60 %	6	2.43	1.160	9.3	0.069
B40	volume 40 %	6	1.63	1.713	13.9	0.064

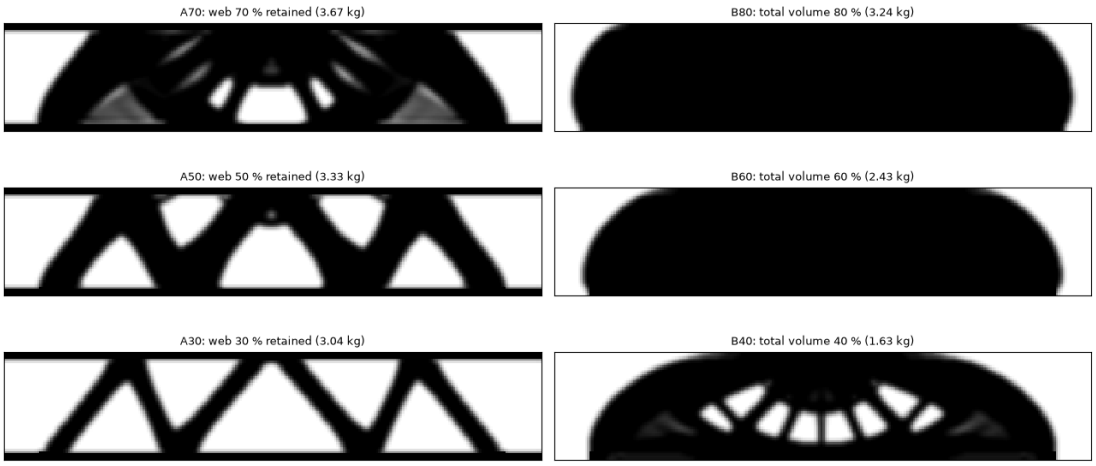


Fig. 5. *Mid-plane of the web for the layouts found. Left: designs with the flanges kept (setup A). Right: designs with the whole section free (setup B). Masses are given in the panel titles.*

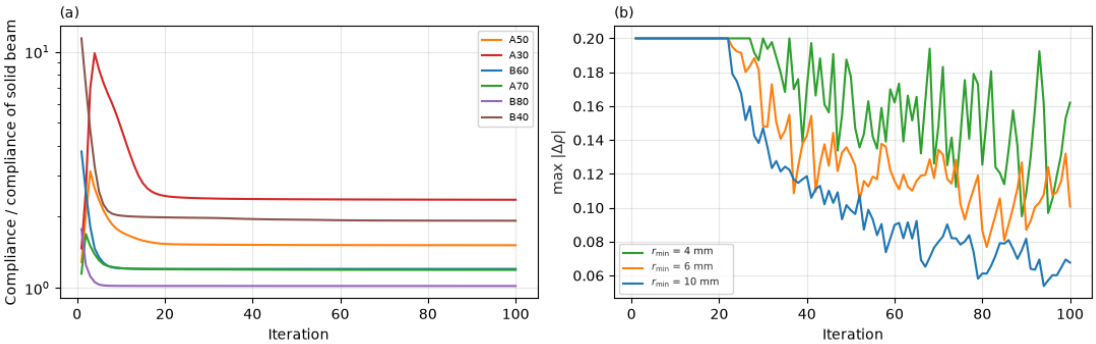


Fig. 6. *Compliance history relative to the solid beam (a) and largest density change (b)*

4. ELASTOPLASTIC FORCE–DISPLACEMENT RESPONSE OF THE DESIGNS

Reading the Curves: Figure 7a shows the force–displacement curves. The displacement is the vertical movement of the load strip at mid-span; the force is the total force on the beam. The force first increases, reaches its largest value and then decreases. The force was evaluated at prescribed displacement steps (for the solid beam and B60 at 0.1, 0.5, 1, 2, 4, 6, 8, 10

and 12 mm); the largest force is the largest of these sampled values, and the displacement at which it occurs is known only to the step size. In Table 4 the force is that of the full beam. First yield is the displacement at which yielding starts under the load strip (step 0.1 mm). ε_p is the largest equivalent plastic strain at 4 mm under the load strip and elsewhere; the location of the latter is given as distance from mid-span. Residual deflection is the displacement that remains after unloading from 4 mm. The 12 mm values are indicative.

Solid Beam: The largest force of the solid beam is 93.9 kN (at 4 mm); at 12 mm it carries 62.7 kN. The largest force is 70 % of the plastic hinge load of the closed form (133.5 kN). Plastic strain concentrates under the load strip (Figure 8); this points to crushing of the web and indentation of the flange under the strip rather than to a fully developed plastic hinge. Since the material model has positive hardening, the later decrease of the force is of geometric origin; it is attributed to local crippling of the web under the load and to the change of the section shape, which were not examined separately.

B60: B60 (2.43 kg, 40 % lighter) reaches 92.7 kN at 4 mm, which is 99 % of the solid beam. At 12 mm it carries 53.2 kN (85 %). The largest force per unit mass is 38.2 kN/kg (23.2 for the solid beam).

A50: A50 (3.33 kg, 18 % lighter) reaches 70.0 kN at 2 mm, which is 74 % of the solid beam (21.0 kN/kg). The force then falls to 46.4 kN at 4 mm (49 % of the solid beam) and to 27.2 kN at 12 mm (43 %). While the linear stiffness loss is only 31 % (compliance ratio 1.45), the force loss at 4 mm is 51 %; linear compliance thus understates the loss of capacity of A50 in the plastic range. A point on the curve at 5.5 mm (52.0 kN) does not agree with its neighbours (38.2 and 34.6 kN); it was regarded as a probable numerical error and left out of the curve, the energy and the tables; its cause was not examined further, and the values of A50 after the largest force are indicative.

A30: A30 (3.04 kg) reaches 41.4 kN at 1 mm; the force at 4 mm is 32.6 kN. The analysis stopped at 5.5 mm because elements in the thin diagonals became distorted. The values of this design after the largest force depend on the load step sequence and are indicative only.

Energy: The energy absorbed up to 12 mm (area under the curve, Figure 7b) is 925 J for the solid beam, 843 J for B60 and 476 J for A50, or 228, 347 and 143 J/kg. Up to 4 mm the values are 295, 285 and 218 J.

Residual Deflection: When the load is reduced from 4 mm to zero, all designs keep a residual deflection of 2.9–3.1 mm (Table 4); about 1 mm recovers elastically. The differences between the designs are within 0.2 mm.

Table 4. *Elastoplastic response of the designs.*

Design	Mass (kg)	First yield (mm)	F at 4 mm (kN)	Largest F (kN) / displ. (mm)	F at 12 mm (kN)	ε_p at 4 mm (largest): under load / elsewhere	Location of largest ε_p outside the load strip	Residual deflection (mm)
Solid IPE100	4.05	0.2	93.9	93.9 / 4.0	62.7	0.30 / 0.09	web, 0 mm	3.04
B60	2.43	0.2	92.7	92.7 / 4.0	53.2	0.28 / 0.07	web, 0 mm	2.90
A50	3.33	0.3	46.4	70.0 / 2.0	27.2	0.13 / 0.07	web, 187 mm	3.10
F-A	3.49	0.3	77.4	77.4 / 4.0	39.0	0.18 / 0.06	web, 16 mm	2.90
F-B	2.51	0.2	90.9	90.9 / 4.0	–	0.27 / 0.07	web, 215 mm	2.93
A30	3.04	–	32.6	41.4 / 1.0	–	0.01 / 0.08	web, 170 mm	–

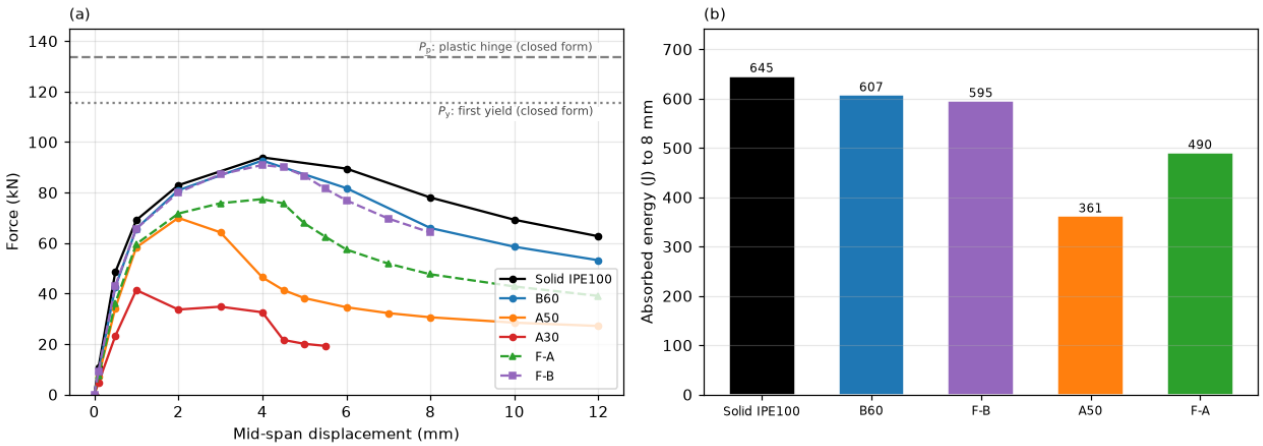


Fig. 7. *Force–displacement curves (a) and absorbed energy (b); the force is that of the full beam*

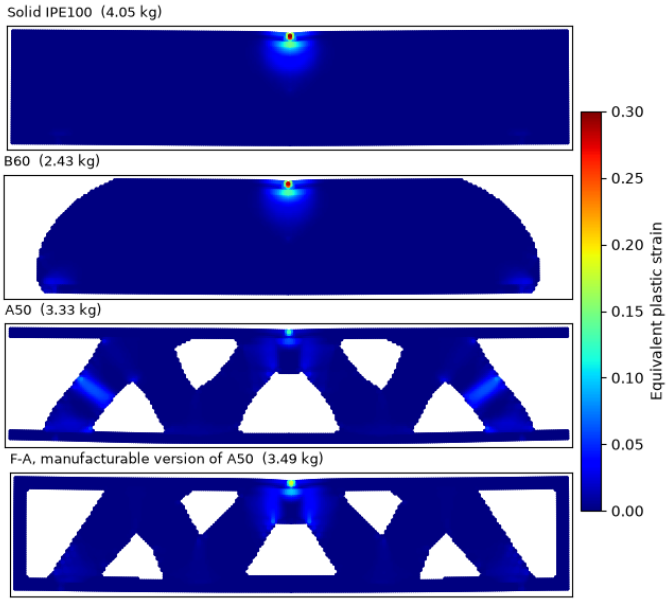


Fig. 8. *Equivalent plastic strain at 4 mm displacement of the load strip (mid-plane of the web, mirrored about mid-span): solid beam, topology designs B60 and A50, and the manufacturable design F-A*

5. BUCKLING CHECK OF THE DIAGONALS

Method: The diagonals in A50 and A30 are thin plates of 4.1 mm thickness; their out-of-plane buckling is a possible reason for the loss of force after the largest force. As a rough check, the Euler buckling load of a strut ($P_{cr} = \pi^2 EI/L^2$, $I = wt^3/12$) was calculated. The strut width w is twice the median distance from the centre line of the material skeleton to the boundary; the length L = 102 mm follows from an inclination of 60° over the web height; the axial force in one diagonal was taken as $F/(2\sin 60°)$. The inclination, the length and the widths were estimated from the layout, so the calculation is an order-of-magnitude check only; the diagonals are plates connected to the flanges and to neighbouring regions, not isolated struts (Table 5).

Result: For A50 the Euler load with pinned ends is 40 kN, against a strut force of 40 kN at the largest force; for A30 the values are 23 and 24 kN. The two values are of the same order; with fixed ends the Euler load would be four times larger. The real end condition lies between the two. At the largest force the axial stress in the struts is about 280 MPa in both designs, close to the yield strength, so yielding and buckling

interact and the elastic Euler load is an upper bound. Buckling of the diagonals therefore cannot be excluded, but the mechanism was not proven in this study; the finite element models contain no initial geometric imperfection and are therefore not expected to represent out-of-plane buckling reliably.

Table 5. *Rough Euler check of the diagonals (L = 102 mm, 60° inclination assumed).*

Design	Median strut width (mm)	Euler load, pinned ends (kN)	Euler load, fixed ends (kN)	Largest force (kN)	Strut force at that force (kN)
A50	34.8	39.6	158.3	70.0	40.4
A30	20.5	23.3	93.3	41.4	23.9

6. MESH CONVERGENCE

Dividing each element into eight (1.025 mm) gave forces that were compared with the original 2.05 mm mesh (Figure 9): B60: 97.0 kN (fine mesh) and 92.7 kN (coarse mesh) at 4.0 mm, difference +4.7 %; A50: 57.5 kN (fine mesh) and 65.2 kN (coarse mesh) at 3.0 mm, difference −11.7 %. F-A: 79.0 kN (fine mesh) and 77.4 kN (coarse mesh) at 4.0 mm, difference +2.1 %. Up to the largest force, the fine mesh gives a 2–6 % higher force; the largest force thus changes by less than about 6 % with mesh refinement. The refinement keeps the stepped boundary of the voxel model; it tests the discretisation, not the representation of the geometry. In the refined model the displacement acts on three node rows (a loaded width of about 3.1 mm instead of 2.05 mm), so the effect of the element size and that of the loaded width are not separated. After the largest force the difference grows: the fine-mesh analysis of A50 stopped at 3 mm because elements were distorted, and there the force is 12 % below the coarse mesh. The behaviour after the largest force therefore depends on the mesh. No mesh check was made for F-B.

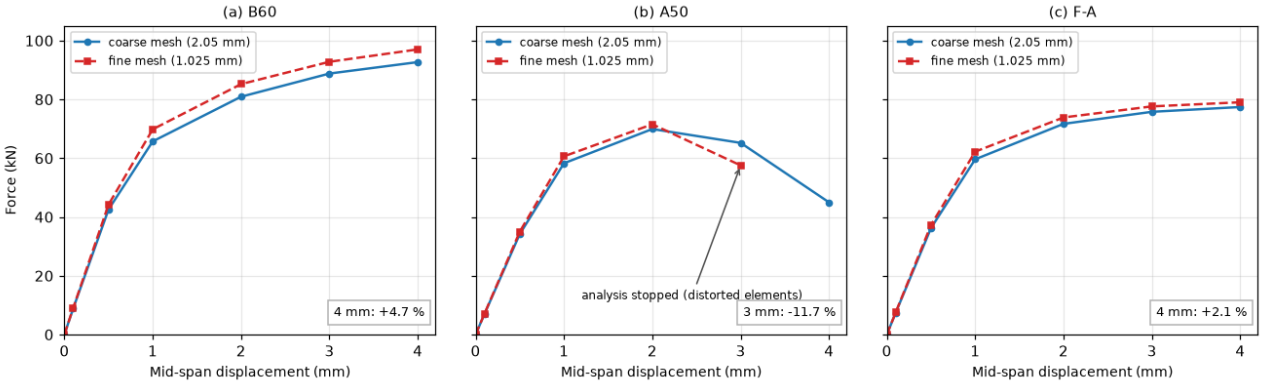


Fig. 9. *Force–displacement curves with the original (coarse) and the refined (fine) mesh for B60 (a), A50 (b) and F-A (c); the percentages give the difference of the fine mesh at the last common displacement.*

7. MANUFACTURABLE DESIGNS

Motivation: The edges of the topology optimisation output are irregular and cannot be manufactured as they are. A manufacturable design was derived from each of the two layouts (Figure 10).

F-A: F-A is a rolled IPE100 with seven web openings that follow A50. Derivation steps: the density field in the web mid-plane was smoothed, its 0.5 contour was converted to polygons, each polygon was reduced to 3–5 straight edges, ligaments thinner than 8 mm were closed, corners were rounded to a radius of 4 mm, and an end post of 8 mm was kept at both ends of the beam. The openings are cut by laser (cut length 1.42 m, removed web area 17 589 mm^2). The flanges and the section are those of the rolled profile, and no welding is needed.

F-B: F-B follows B60 as a tapered beam welded from three laser-cut plates (web 4.1 mm, flanges 5.7 mm). The web height rises from 46 mm at the end to 86 mm and, 104 mm from the end, to 100 mm; the top flange widens from 8 mm and the bottom flange from 17 mm to 55 mm towards mid-span. All contours are straight lines. The girder is 436 mm long for a span of 420 mm; relative to a solid IPE100 of the same length (3.53 kg), its mass is 29 % lower, so part of the 38 % reduction comes from the shorter overhangs.

Analysis Results: The two designs were analysed with the model of the previous sections (Table 4 and Table 6). F-A (3.49 kg, 14 % lighter than the solid beam) reaches 77.4 kN, 82 % of the solid beam; for A50 the value is 70.0 kN. F-B (2.51 kg, 38 % lighter) reaches 90.9 kN, 97 % of the solid beam; for B60 it is 92.7 kN. The largest force per unit mass is 22.2 kN/kg for F-A, 36.2 for F-B and 23.2 for the solid beam. F-A thus saves mass relative to the solid beam, while its force per unit mass is close to that of the solid beam; the difference (4 %) is smaller than the mesh dependence (about 6 %) and depends on the mass basis (see below). F-B raises the force per unit mass. The analysis of F-B ended at 8.0 mm and did not reach 12 mm. In F-A, plastic strain concentrates under the load strip and at the foot of the diagonals (Figure 8).

Files: STEP models of both designs and DXF cut patterns were prepared. The CAD masses are 3.32 kg for F-A and 2.44 kg for F-B, below the masses of the finite element model (3.49 and 2.51 kg); the root fillets of the IPE100 are not modelled in the CAD files, and the surfaces of the finite element model have stair steps. The CAD geometries were not analysed; if the force of F-A were unchanged, the CAD mass would give 23.3 kN/kg, so the comparison with the solid beam depends on the mass basis.

Table 6. *Manufacturable designs F-B and F-A against the topology designs B60 and A50 and the solid beam (ANSYS, same model; mass from the finite element model). Force and energy are given over the same displacement range (8 mm, where the analysis of F-B ends) for all designs*

Design	Mass (kg)	Largest force (kN)	F at 8 mm (kN)	Energy to 8 mm (J)	Largest force / mass (kN/kg)
Solid IPE100	4.05	93.9	78.0	645	23.2
B60	2.43	92.7	65.9	607	38.2
F-B	2.51	90.9	64.2	595	36.2
A50	3.33	70.0	30.6	361	21.0
F-A	3.49	77.4	47.6	490	22.2

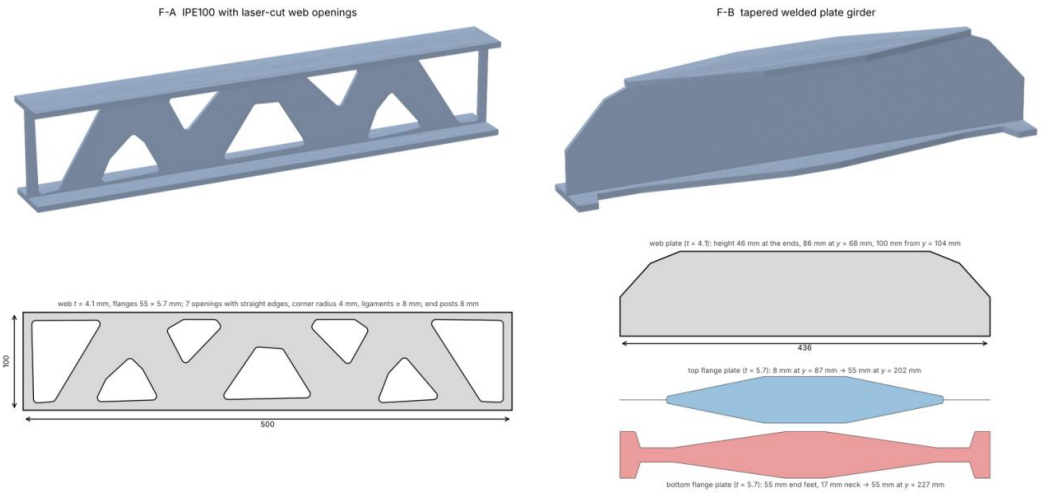


Fig. 10. *Manufacturable designs: F-A, derived from A50, an IPE100 with seven straight-edged laser-cut web openings; F-B, derived from B60, a tapered girder welded from three plates (dimensions in mm)*

8. COST

Inputs: The cost was estimated as the extra processing cost per piece relative to the solid IPE100. The inputs are project assumptions: S355 at 0.764 EUR/kg (material of the solid beam 3.09 EUR), scrap at one third of the steel price (0.25 EUR/kg), laser cutting at 0.6 EUR/m and welding at 1.16 EUR/m. A Master's thesis reports laser cutting costs of 0.14 EUR/m for one company, with plasma at 0.21 and oxy-fuel at 0.25 EUR/m [30]. A plate price of about 950 EUR per tonne has been reported [31]. No data are available for piercing, set-up and fixturing costs, the weld size was not defined, and these items were not included.

Calculation: Cutting openings into a rolled section removes steel that was bought with the section; the removed mass is not a saving, it returns only as scrap. The extra cost of F-A is therefore the cutting cost minus the scrap revenue (Eq. 8). F-B is made of plates, so less steel is bought; its extra cost is the cutting and welding cost plus the material difference (Eq. 9).

$$\Delta C_{\mathrm{A}} = c_{\mathrm{cut}}\ell_{\mathrm{cut}} - c_{\mathrm{scrap}}m_{\mathrm{rem}} \tag{8}$$

$$\Delta C_{\mathrm{B}} = c_{\mathrm{cut}}\ell_{\mathrm{plate}} + c_{\mathrm{weld}}\ell_{\mathrm{weld}} - c_{\mathrm{steel}}(m_{\mathrm{solid}} - m_{\mathrm{B}}) \tag{9}$$

Result: The seven openings of F-A have a cut length of 1.42 m and remove 0.57 kg. The cutting costs 0.85 EUR and the scrap returns 0.14 EUR; the net extra cost is 0.71 EUR (23 % of the material cost of the solid beam). The plate contours of F-B need 2.73 m of cutting and 1.52 m of welding: cutting 1.64 EUR, welding 1.76 EUR, material saving 1.18 EUR; the net extra cost is 2.22 EUR (72 %; Table 7). Relative to a solid IPE100 of the same length (436 mm), the material saving would be 0.78 EUR and the net extra cost 2.62 EUR. Per kilogram of mass saved, the extra cost is 1.26 EUR/kg for F-A and 1.44 EUR/kg for F-B. The material item of F-B does not include plate waste; the real cost is therefore higher. With the laser cutting price of 0.14 EUR/m reported in [30], the extra cost would be 0.05 EUR for F-A and 0.97 EUR for F-B; the order of the two designs does not change.

Table 7. *Extra cost per piece relative to the solid IPE100 (steel 0.764 EUR/kg, scrap 0.25 EUR/kg, cutting 0.6 EUR/m, welding 1.16 EUR/m; piercing, set-up and plate waste not included)*

Design	Mass (kg)	Cutting (EUR)	Welding (EUR)	Scrap / material (EUR)	Net extra cost (EUR)	Per kg saved (EUR/kg)
F-A (rolled, 7 openings)	3.49	0.85	–	−0.14	+0.71	+1.26
F-B (welded plates)	2.51	1.64	1.76	−1.18	+2.22	+1.44

9. DISCUSSION

The main finding is that, under the loading and load-strip model studied, the effect of lightening on the largest computed reaction force depends on the layout. B60 removes 40 % of the material and reaches 99 % of the largest force of the solid beam; A50 is 18 % lighter and loses 26 % of the force (Table 4). Because the largest force of the solid beam is limited by local yielding under the load strip, which is kept in all designs, this comparison refers to the load introduction used here. Linear compliance understates this difference: the stiffness loss of A50 is 31 %, while its force loss at 4 mm is 51 %. This is consistent with the literature: designs obtained with a linear and a nonlinear model are similar unless buckling or snap-through occurs [22], and formulations that account for plasticity or stress directly give layouts that carry more load up to yielding than minimum-compliance layouts [25]. The layouts used here are minimum-compliance solutions. In B60 the flanges stay where the bending resistance is needed, whereas in A50 the load is carried by thin diagonals. The rough Euler check shows that the buckling load of

the diagonals is of the same order as the strut force at the largest force, so buckling of the diagonals is a possible factor, but the mechanism was not proven here. If plasticity [24,25], stress [26] or buckling [27] is constrained directly, this loss could be addressed at the design stage.

Plastic strain concentrates under the load strip and, in F-A, at the foot of the diagonals (Figure 8). In perforated beams with large openings, Vierendeel bending is the usual critical mechanism [2,3]; the local plasticity at the diagonal feet is thought to be similar to it, but separating it from plasticity at the strut ends would need a separate study. Earlier work on topology optimisation of I-sections with openings compared the results with cellular beams [13,14]; here the reference is the solid beam. Topology optimisation of I-beams for plastic-limit behaviour has also been studied for various beam–column connections [32].

F-A is 0.16 kg heavier than A50 and carries more force (77.4 kN against 70.0 kN for A50); the effect of the mass and that of the contour were not separated. The force per unit mass of F-A (22.2 kN/kg) is close to that of the solid beam (23.2 kN/kg); the difference lies within the mesh and mass uncertainties. For this loading, cutting web openings into a rolled beam therefore reduced the mass without a measurable gain in force per unit mass. The force per unit mass of F-B (36.2 kN/kg) is 56 % higher than that of the solid beam; if the force of a 436 mm solid beam is taken as unchanged, the difference is about 36 %. F-B is a tapered girder whose depth and flange width follow the bending moment; part of this gain is expected from the tapering itself, and since a conventionally tapered girder of equal mass was not analysed, the contribution of the topology optimisation was not separated. Converting a topology result to a manufacturable design by a separate step has also been done for vehicle parts: a suspension cap [18], a suspension arm [19] and a brake pedal [17]. The conversion here is geometric (smoothing, polygonisation, ligaments of at least 8 mm).

F-A costs 0.71 EUR and F-B 2.22 EUR more than the solid beam (Table 7). For F-A, the extra cost arises because the steel removed from the rolled section returns only at scrap value; F-B buys less steel but needs cutting and welding. The cost results depend on the unit price assumptions; piercing, set-up and plate waste are not included. Cellular beams have been criticised for their fabrication cost because they need two cuts along the web [1]. For lightening to save cost, the processing cost paid per kilogram of steel removed must be lower than the price of the steel. In F-A, 0.85 EUR of cutting was paid for 0.57 kg removed (about 1.5 EUR/kg); since the removed steel has already been bought and returns only at scrap value, cutting openings into a rolled beam cannot reduce its cost. In F-B, the steel not bought is worth 1.18 EUR, and cutting and welding cost 3.40 EUR (about 2.2 EUR per kilogram removed). With the unit prices used, the condition is not met by either design.

The limitations of the study are as follows: (i) The load is applied to one node row (about 2.05 mm) and each support to two node rows (about 4.1 mm), and the support plates were not modelled; the Hertz estimate shows that the real contact is plastic and widens, and the forces reported are those of this load introduction. The largest force of the solid beam (93.9 kN) is below the closed-form first-yield load (115.9 kN), and plastic strain concentrates under the load strip, which is the same in all designs; the largest forces therefore reflect the local resistance under the strip to a large extent, and the effect of the strip width was not studied. (ii) The hardening modulus ($E/100$) is an assumption, and the behaviour after the largest force depends on it. (iii) The topology runs ended at 100 iterations without reaching the stopping criterion; the layouts are not exact optima. (iv) The values at 12 mm are indicative; the plastic strain under the strip is large. (v) The analysis of F-B ended at 8 mm and no mesh check was made. (vi) The models contain no initial geometric imperfection,

so out-of-plane buckling of the diagonals is not reliably represented. (vii) One short beam (span-to-depth ratio 4.2) and one loading case were studied, and there is no experimental validation; the results cannot be transferred directly to longer beams with web openings.

CONCLUSIONS

1. Under the loading and load-strip model studied, the effect of lightening depends on where the material is removed. B60, in which the whole section including the flanges changes, reached 99 % of the largest computed reaction force of the solid beam with 40 % of the material removed; A50, in which material is removed from the web only, is 18 % lighter and reached 74 %. Linear compliance understated this difference.

2. The largest force per unit mass (kN/kg) is 23.2 for the solid beam, 38.2 for B60, 21.0 for A50, 22.2 for F-A and 36.2 for F-B.

3. F-A, a rolled IPE100 with seven laser-cut web openings, reduced the mass by 14 % and kept 82 % of the force; its force per unit mass is close to that of the solid beam. Its extra cost is 0.71 EUR per piece. Since the removed steel returns only at scrap value, the cost cannot be reduced in this way.

4. F-B, a tapered girder welded from three plates, reduced the mass by 38 % (29 % relative to a solid beam of the same length), kept 97 % of the force and raised the force per unit mass. Because cutting and welding (3.40 EUR) cost more than the steel not bought (1.18 EUR), its extra cost is 2.22 EUR. Its analysis ended at 8 mm, and the gain was not separated from that of conventional tapering.

5. Lightening by topology optimisation saves cost only when the processing cost paid per kilogram of steel removed is lower than the price of the steel. With the unit prices used, this condition is not met by either design; the lightening is worthwhile where the mass reduction has a value of its own in use.

6. The results hold for the beam, the load applied to one node row and the loading studied, with the assumed material model ($E/100$) and unit prices; the topology runs ended at the iteration limit.

DECLARATION OF GENERATIVE AI USE

The author used an AI tool to transfer the analysis results into graphs and to edit the text. The author reviewed the content and takes full responsibility for it.

REFERENCES

[1] A. Kaveh, A. Fakoor, “Cost Optimization of Steel-concrete Composite Floor Systems with Castellated Steel Beams,” Periodica Polytechnica Civil Engineering, vol. 65, no. 2, pp. 353–375, 2021.

[2] K. D. Tsavdaridis, C. D’Mello, “Vierendeel Bending Study of Perforated Steel Beams with Various Novel Web Opening Shapes, through Nonlinear Finite-Element Analyses,” Journal of Structural Engineering, vol. 138, no. 10, pp. 1214–1230, 2012.

[3] K. D. Tsavdaridis, C. D’Mello, “Optimisation of novel elliptically-based web opening shapes of perforated steel beams,” Journal of Constructional Steel Research, vol. 76, pp. 39–53, 2012.

[4] M. P. Bendsøe, N. Kikuchi, “Generating optimal topologies in structural design using a homogenization method,” Computer Methods in Applied Mechanics and Engineering, vol. 71, no. 2, pp. 197–224, 1988.

[5] M. P. Bendsøe, “Optimal shape design as a material distribution problem,” Structural Optimization, vol. 1, no. 4, pp. 193–202, 1989.

[6] M. P. Bendsøe, O. Sigmund, Topology Optimization: Theory, Methods and Applications, Springer, Berlin, 2003.

[7] O. Sigmund, K. Maute, “Topology optimization approaches: A comparative review,” Structural and Multidisciplinary Optimization, vol. 48, no. 6, pp. 1031–1055, 2013.

[8] O. Sigmund, J. Petersson, “Numerical instabilities in topology optimization: A survey on procedures dealing with checkerboards, mesh-dependencies and local minima,” Structural Optimization, vol. 16, no. 1, pp. 68–75, 1998.

[9] B. Bourdin, “Filters in topology optimization,” International Journal for Numerical Methods in Engineering, vol. 50, no. 9, pp. 2143–2158, 2001.

[10] O. Sigmund, “A 99 line topology optimization code written in Matlab,”

Structural and Multidisciplinary Optimization, vol. 21, no. 2, pp. 120–127, 2001.
[11] E. Andreassen, A. Clausen, M. Schevenels, B. S. Lazarov, O. Sigmund, "Efficient topology optimization in MATLAB using 88 lines of code," Structural and Multidisciplinary Optimization, vol. 43, no. 1, pp. 1–16, 2011.
[12] K. Liu, A. Tovar, "An efficient 3D topology optimization code written in Matlab," Structural and Multidisciplinary Optimization, vol. 50, no. 6, pp. 1175–1196, 2014.
[13] J. J. Kingman, K. D. Tsavdaridis, V. V. Toropov, "The Application of Topology Optimisation to the Design of Steel I-Section Beam Web Openings," Civil-Comp Proceedings, vol. 102, paper 223, 2013.
[14] K. D. Tsavdaridis, J. J. Kingman, V. V. Toropov, "Application of structural topology optimisation to perforated steel beams," Computers & Structures, vol. 158, pp. 108–123, 2015.
[15] A. R. Yildiz, N. Kaya, F. Ozturk, O. Alankus, "Optimal design of vehicle components using topology design and optimisation," International Journal of Vehicle Design, vol. 34, no. 4, pp. 387–398, 2004.
[16] A. R. Yıldız, U. A. Kılıçarpa, E. Demirci, M. Doğan, "Topography and topology optimization of diesel engine components for light-weight design in the automotive industry," Materials Testing, vol. 61, no. 1, pp. 27–34, 2019.
[17] E. Kurt, A. R. Yıldız, T. İnkaya, A. R. Özcan, İ. Gökdağ, "Lightweight design of lattice-embedded brake pedals using artificial intelligence-based optimization," Materials Testing, vol. 68, no. 1, pp. 83–95, 2026.
[18] G. Karadere, Y. Düzcan, A. R. Yıldız, "Light-weight design of automobile suspension components using topology and shape optimization techniques," Materials Testing, vol. 62, no. 5, pp. 454–458, 2020.
[19] B. Aslan, A. R. Yıldız, "Optimum design of automobile components using lattice structures for additive manufacturing," Materials Testing, vol. 62, no. 6, pp. 633–639, 2020.
[20] A. R. Yildiz, "Optimal Structural Design of Vehicle Components Using Topology Design and Optimization," Materials Testing, vol. 50, no. 4, pp. 224–228, 2008.
[21] A. R. Yildiz, N. Öztürk, N. Kaya, F. Öztürk, "Integrated optimal topology design and shape optimization using neural networks," Structural and Multidisciplinary Optimization, vol. 25, no. 4, pp. 251–260, 2003.
[22] T. Buhl, C. B. W. Pedersen, O. Sigmund, "Stiffness design of geometrically nonlinear structures using topology optimization," Structural and Multidisciplinary Optimization, vol. 19, no. 2, pp. 93–104, 2000.
[23] T. E. Bruns, D. A. Tortorelli, "Topology optimization of non-linear elastic structures and compliant mechanisms," Computer Methods in Applied Mechanics and Engineering, vol. 190, no. 26–27, pp. 3443–3459, 2001.
[24] K. Maute, S. Schwarz, E. Ramm, "Adaptive topology optimization of elastoplastic structures," Structural Optimization, vol. 15, no. 2, pp. 81–91, 1998.
[25] O. Amir, "Stress-constrained continuum topology optimization: a new approach based on elasto-plasticity," Structural and Multidisciplinary Optimization, vol. 55, no. 5, pp. 1797–1818, 2017.
[26] C. Le, J. Norato, T. Bruns, C. Ha, D. Tortorelli, "Stress-based topology optimization for continua," Structural and Multidisciplinary Optimization, vol. 41, no. 4, pp. 605–620, 2010.
[27] X. Gao, H. Ma, "Topology optimization of continuum structures under buckling constraints," Computers & Structures, vol. 157, pp. 142–152, 2015.
[28] EN 10025-2, Hot rolled products of structural steels – Part 2: Technical delivery conditions for non-alloy structural steels.
[29] K. L. Johnson, Contact Mechanics, Cambridge University Press, Cambridge, 1985.
[30] N. Wells, "Techno-economical comparison of cutting metal sheets with plasma, oxy-fuel and laser technologies," Master thesis, Tallinn University of Technology, 2024.
[31] Eurometal, "Northwest European plate prices to inch up," 16 January 2023, https://eurometal.net/northwest-european-plate-prices-to-inch-up/
[32] P. Grubits, R. Cucuzza, M. Habashneh, M. Domaneschi, P. Aela, M. Movahedi Rad, "Structural topology optimization for plastic-limit behavior of I-beams, considering various beam-column connections," Mechanics Based Design of Structures and Machines, 2024, doi: 10.1080/15397734.2024.2412757.